This article has been accepted for publication in IEEE Sensors Journal. This is the author's version which has not been fully edited and content may change prior to final publication. Citation information: DOI 10.1109/JSEN.2024.3374817



# Ultra-Miniaturized Dual-Band Implantable Antenna for Wireless Capsule Endoscopy

Abdullah Alshammari, *Student Member, IEEE*,Amjad Iqbal, *Member, IEEE*,Abdul Basir, *Member, IEEE*,Roy B. V. B. Simorangkir *Member, IEEE*, Ismail Ben Mabrouk, *Senior Member, IEEE*

***Abstract*— This study introduces a small dual-band implantable antenna designed for Wireless Capsule Endoscopy (WCE). This antenna operates in the Wireless Medical Telemetry Service (WMTS) 1.4 GHz as well as the Industrial, Scientific, and Medical (ISM) 2.45 GHz bands. The designed antenna achieves miniaturization by employing open-ended slots, shorting pins, and arc-shaped slots on the radiating patch. The final structure has a compact size of 8.2 x 8.2 x 0.635 mm$^3$. Homogeneous muscle and heterogeneous human phantoms are used to analyze the antenna's behavior. The measurements are conducted by implanting the WCE device within minced pork meat. Considering the capsule's deep location, the proposed antenna achieves gain values of -29.4 dBi at 1.4 GHz and -30.4 dBi at 2.45 GHz, respectively. The measured impedance bandwidths are 7.2 % and 4.2 % at 1.4 GHz and 2.45 GHz, respectively. Results suggest that the proposed antenna can reliably establish wireless communication at distances greater than 10 meters with a 10 dB margin for both frequencies. The 10-g specific absorption rate (SAR) values are 4.77 W/kg and 6.07 W/kg at 1.4 GHz and 2.45 GHz, respectively.**

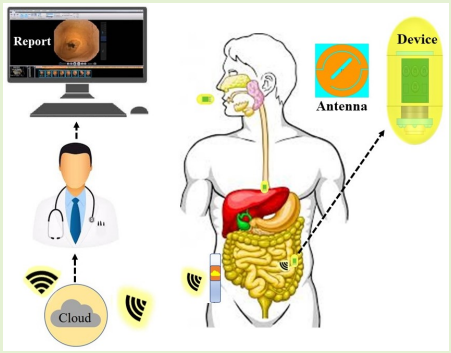


***Index Terms*— Biomedical, compact implantable antenna, dual-band, wireless capsule endoscopy applications.**

## I. Introduction

THE Wireless Capsule Endoscopy (WCE) represents a leading-edge diagnostic method that revolutionizes the visualization of the gastrointestinal tract [1]. Recently, this innovative technology has gained significant attention owing to its non-invasive and painless approach, presenting a highly appealing alternative to traditional wired endoscopic procedures [2], [3]. Conventional endoscopy, as the current gold standard, is characterized by its invasive and discomforting nature when used to examine the GI tract. Moreover, it has intrinsic limitations, including its inability to provide a comprehensive view of the small intestine [4]. The core structure of WCE lies in the integration of key components, as showcased in Fig. 1. Within the biocompatible shell, a WCE typically integrates an antenna, camera, light-emitting diodes (LEDs), batteries, sensors, and printed circuit board (PCB) [5], [6]. Among these components, the antenna holds a pivotal role in enabling wireless communication, serving as the communication bridge between the capsule and the external receivers. Researchers have explored various avenues

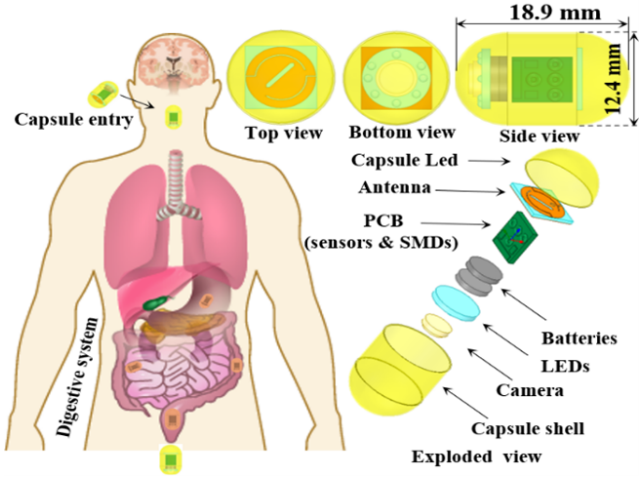


Fig. 1. An overview of the WCE scenario, including the capsule architecture

to address the complex challenges associated with the antennas for such a complex working environment within the human body. One key area of focus has been the quest for miniaturized antennas with dual-band performance, which represents a formidable engineering challenge, owing to the capsule dimensions constraints.

Dual-band antennas are of particular interest, given their ability to operate on two distinct frequency bands. This feature is important for implantable applications, including wireless capsule endoscopy, as it allows simultaneous transmission of

Manuscript received 1 February 2024. (Corresponding author: Abdullah Alshammari.) This work was supported by the Royal Society under Newton International Fellowship (Grant Number: NIF\R1\221500).
Abdullah Alshammari, Amjad Iqbal, Abdul Basir, Roy B. V. B. Simorangkir and Ismail Ben Mabrouk are with the Department of Engineering, Durham University, Durham DH1 3LE, U.K. (e-mail: Abdullah.h.alshammari@durham.ac.uk; amjad730@gmail.com; roy.b.simorangkir@durham.ac.uk; ismail.benmabrouk@durham.ac.uk). A. Basir is with the Faculty of Information Technology and Communication Sciences, Tampere University, Finland (Email: abdul.basir@tuni.fi).

© 2024 IEEE. Personal use is permitted, but republication/redistribution requires IEEE permission. See https://www.ieee.org/publications/rights/index.html for more information.

This article has been accepted for publication in IEEE Sensors Journal. This is the author's version which has not been fully edited and
content may change prior to final publication. Citation information: DOI 10.1109/JSEN.2024.3374817



data and reception on separate frequency bands. This simultaneous dual-band operation enhances communication reliability and flexibility within the human body, optimizing the overall performance of implantable devices [7], [8]. In wireless capsule endoscopy, a dual-band antenna is crucial to enable simultaneous data transmission and wireless power transfer. Designing such an antenna ensures efficient communication and sustained power supply, optimizing the functionality and longevity of the capsule within the body [9].

Several strategies are employed to achieve antenna miniaturization in the dual-band context. Techniques such as defective ground layers [10] and the utilization of elevated dielectric substrates [11] have been investigated. Achieving miniaturization presents a unique challenge as it directly affects both antenna gain and bandwidth, requiring a trade-off. In the pursuit of dual-band antennas, researchers have explored creative designs and solutions. Using a meander-line structure, a dual-band compact antenna is described in [12]. The device operates at 1.4 GHz and 2.4 GHz. However, it has a large dimension (10 x 10 x 0.635 $mm^3$). An implanted dual-band antenna that operates in the ISM band is described in [13]. It has a volume of 22 × 16 × 1.27 $mm^3$, however, the antenna's dimensions are not suitable for WCE applications due to its rigid and non-conformal geometry. Additionally, a dual-band implanted antenna for monitoring hyperglycemia that operates at 405 MHz and 2450 MHz has been extensively studied in [14]. Nevertheless, it's worth noting that its size is quite large, measuring 1265.625 $mm^3$. Notable achievements include a compact dual-band design in [15], achieved through the clever integration of slots and shorting pins. In a similar vein, meandered resonators are harnessed to reduce antenna dimensions by enhancing the current path, as documented in [16]. In [17], a dual-band antenna was developed using a combination of a pin, slotted patch, and open-ended ground layer, leading to notable miniaturization. However, these designs, while possessing dual-band capabilities, are hampered by their substantial dimensions, high SAR values, and relatively low gain, rendering them unsuitable for the stringent demands of WCE applications.

This research introduces a miniaturized dual-band antenna designed for WCE systems, enabling operation at both 1.4 GHz and 2.45 GHz. The suggested design has a compact geometry of 8.2 × 8.2 × 0.635 = 42.69 $mm^3$. Miniaturization and dual band are achieved by shorting pins, open-ended slots, semi-circular slots, and a middle slot on the radiator patch. Considering the deep implant location, the proposed antenna offers distinct advantages compared to other dual-band systems, particularly in size, radiation patterns, and reduced SAR.

## II. Proposed Antenna

### A. Simulation Environment

The antenna simulation using Ansys High-Frequency Simulation Software (HFSS) commenced within a cubical homogeneous phantom, measuring 150 × 150 × 150 $mm^3$. The antenna is enclosed within a WCE capsule device of 18.9 mm length and 6.2 mm radius (see Fig. 1), positioned at a depth of 75 mm within the cubical phantom, as illustrated in Fig. 3(a). The phantom was configured to replicate the electrical properties of human muscle tissue at both 1.4 and 2.45 GHz. Specifically, it was set to have a relative permittivity ($\varepsilon_r$) of 54.1 and a conductivity ($\sigma$) of 1.12 S/m at 1.4 GHz, and $\varepsilon_r$ of 52.7 and $\sigma$ of 1.73 S/m at 2.45 GHz [18]. Following the initial simulation, we progressed to a more realistic human torso phantom, a heterogeneous human model within the HFSS simulation. In this configuration, the capsule was positioned within the stomach at an implantation depth of 75 mm, as depicted in Fig. 3(b).

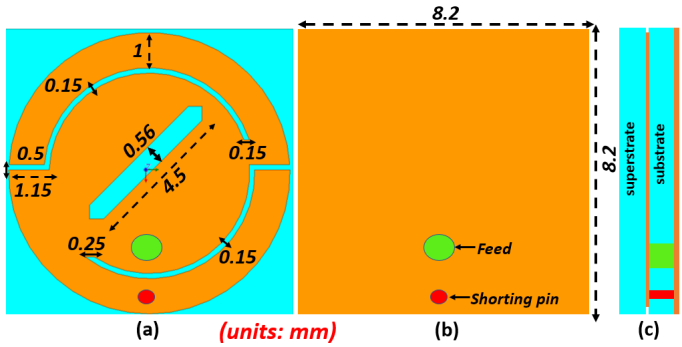


Fig. 2. Geometry of the suggested dual-band antenna: (a) top view, (b) bottom view, and (c) cross-section view.

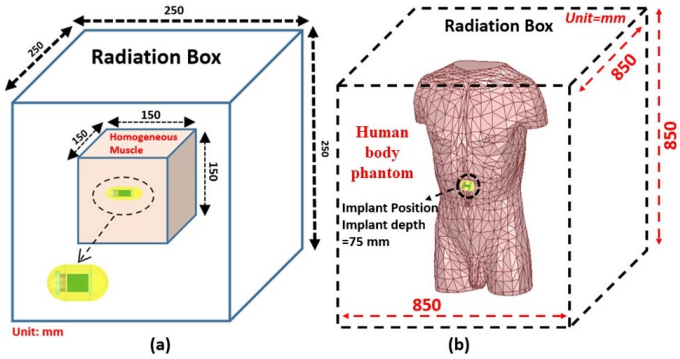


Fig. 3. Antenna simulation setups using (a) cubical homogeneous human muscle phantom and (b) realistic human torso phantom.

### B. Antenna Topology

The suggested antenna takes the form of a circular patch antenna, fed through a 50Ω coaxial probe, with the full ground plane. In order to accomplish the miniaturisation, the design includes a 0.2 mm diameter shorting pin. In addition, semi-circular slots, open-ended slots, and a middle rectangular slot are strategically inserted into the patch to achieve the dual-band characteristic while maintaining compactness. The antenna configuration is presented in Fig. 2 along with its optimized dimensions. Rogers RO3010 material is used for both the antenna's superstrate and substrate, characterized by relative permittivity $\varepsilon_r$ of 10.2 and a low loss tangent (tan $\delta$) of 0.0025, and a thickness of 0.635 mm. To ensure biocompatibility, the capsule enclosure is made of ceramic alumina $Al_2O_3$, which has a thickness of 0.2 mm and a relative permittivity ($\varepsilon_r$) of 9.8.

© 2024 IEEE. Personal use is permitted, but republication/redistribution requires IEEE permission. See https://www.ieee.org/publications/rights/index.html for more information.

This article has been accepted for publication in IEEE Sensors Journal. This is the author's version which has not been fully edited and
content may change prior to final publication. Citation information: DOI 10.1109/JSEN.2024.3374817


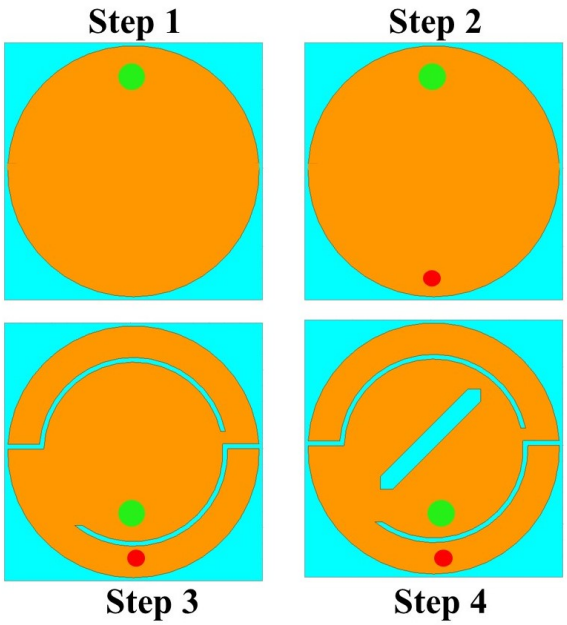


Fig. 4. Antenna design steps

## C. Design Methodology

The suggested dual-band implantable antenna is designed in four major phases, each marked by iterative improvements aimed at optimizing its performance. An overview of these design steps and the corresponding reflection coefficient ($S_{11}$) comparisons can be observed in Figs. 4 and 5, respectively. Throughout these steps, the fundamental patch shape undergoes modifications, while the ground layer remains unchanged. In the initial design step (Step 1), the antenna features a full circular patch, excited by a coaxial probe feed. In this configuration, the antenna resonates at a frequency close to 4.8 GHz. Moving on to Step 2, a crucial modification is introduced by placing a shorting pin within the patch and the ground plane, which is one of the most popular techniques for antenna miniaturization [19]. As a result, the antenna now operates at 1.6 GHz, a significant size reduction of 62%. In Step 3, semi-circular slots and open-ended features are integrated into the radiating patch. This modification enables the antenna to operate in dual-band frequencies, making it more versatile. Additionally, these added openings help reduce the antenna's size while maintaining its dual-band functionality. At this point, the antenna resonates at the frequencies of 1.1 GHz and 2.4 GHz. In the final design step, a rectangular slot is incorporated into the middle of the patch. These refinements serve to align the resonance frequencies with the desired bands. The suggested antenna so displays resonance at 1.4 GHz and 2.45 GHz, effectively achieving its targeted dual-band operation.

## D. Parametric Study

Numerical investigations on the impact of some antenna design parameters on the antenna resonant behavior have been conducted and the results are provided in Figs. 6,7, and 8.

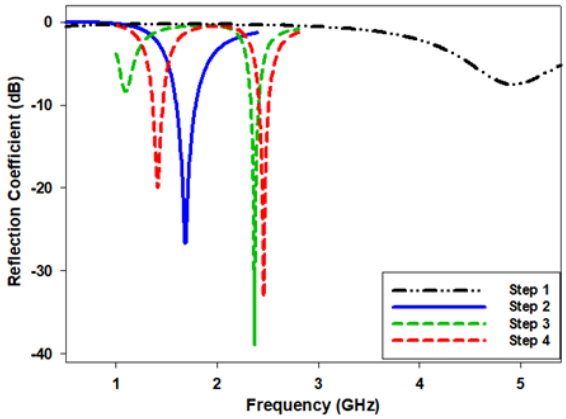


Fig. 5. The antenna reflection coefficient ($S_{11}$) for design steps 1 to 4.

*1) Shorting pin location:* The impact on $S_{11}$ of the suggested antenna owing to differences in the shorting pin position is shown in Fig. 6. The shorting-pin location was systematically varied along the x and y directions, while the feed position remained constant. As a result of field coupling between the feed and the shorting pin, when the pin is placed close to the feed, there is a significant reactance. Conversely, when the shorting pin is positioned farther from the feed, the field coupling is reduced [20]. Shorting pin positions can be varied along the x-axis to achieve the desired resonance frequency, whereas variations along the y-axis have a minimal effect.

*2) Semi-circular Slot Width:* To minimise the overall size of the antenna, semi-circular slots have been inserted into the patch. The impact on $S_{11}$ of the suggested antenna owing to differences in the width of the semi-circular slots within the range of 0.15-0.30 mm is shown in Fig. 7. Notably, this analysis revealed a negligible shift in both frequency bands, indicating that changes in slot width have minimal effect on the resonance characteristics.

*3) Open-end slot Length:* To achieve miniaturization of the antenna size, open-ended slots are added to the radiating patch. Fig. 8 illustrates the effect of varying the length of these open-ended slots, ranging from 0.7 to 1.3 mm, on the antenna's $S_{11}$. Increasing this parameter from 0.7 to 1.3 mm resulted in a substantial shift in both bands' resonance frequency. Specifically, the first band experienced a significant shift from 1.21 to 1.45 GHz, while the second band exhibited a notable shift from 2.25 to 2.65 GHz. Consequently, it was determined that employing open-end slits with a length of 1.15 mm successfully produced resonant frequencies within the desired 1.4 GHz and 2.45 GHz bands.

## E. Current distributions and SAR results

The current distribution of the proposed antenna is depicted in Fig. 9. At 1.4 GHz, there is a noticeable concentration of current around the feeding points. Moreover, the current density is prominently observed along the path extending from the feed to the semi-circular slots located on both the upper and lower sections of the antenna. Similarly, at 2.45 GHz, the currents are primarily focused on the central region of the patch. Furthermore, the current density is higher within the

© 2024 IEEE. Personal use is permitted, but republication/redistribution requires IEEE permission. See https://www.ieee.org/publications/rights/index.html for more information.

This article has been accepted for publication in IEEE Sensors Journal. This is the author's version which has not been fully edited and content may change prior to final publication. Citation information: DOI 10.1109/JSEN.2024.3374817



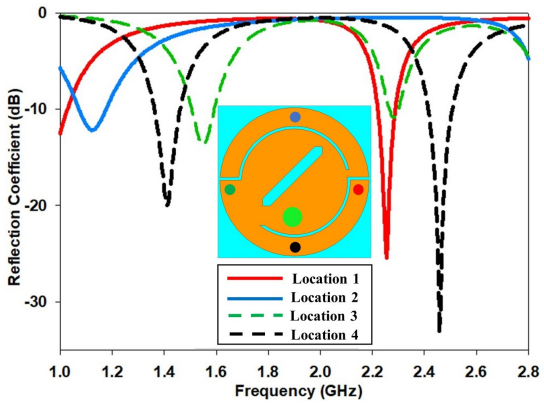


Fig. 6. Effects of the shorting pin location

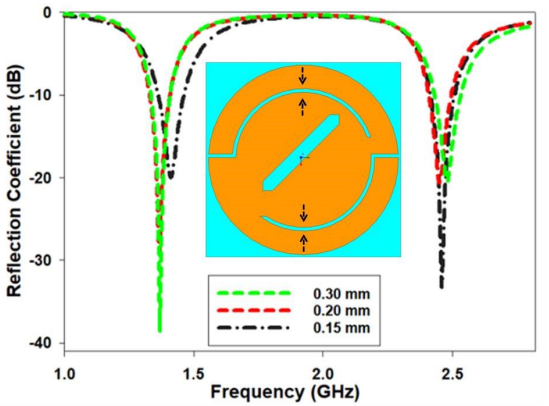


Fig. 7. Effects of the semi-circular slots widths

TABLE I
CALCULATED PEAK SAR (1 W INPUT POWER) AND CORRESPONDING ALLOWABLE MAXIMUM INPUT POWERS

| Frequency (MHz) | Phantom type | SAR (W/kg) 1-g | SAR (W/kg) 10-g | Max allowable power (mW) 1-g | Max allowable power (mW) 10-g |
|---|---|---|---|---|---|
| 1400 | Human Body | 84.8 | 4.77 | 18.86 | 419 |
| 2450 | | 123.7 | 6.07 | 12.93 | 329 |

middle slot and on the right side of the semi-circular slots on the patch. Additionally, significant current density can be observed around the feeding and shorting pin locations for both resonant frequencies.

Assessing the SAR is a crucial element in ensuring the safety of patients when utilizing an in-body WCE. In line with the updated IEEE C95.1-2019 standard, the maximum 10 g averaged SAR value is restricted to 2 W/kg [21]. To perform the SAR evaluations, the human torso phantom with the capsule implanted, as depicted in Fig. 10, is employed. It is important to note that these analyses are conducted with an input power of 1 W applied to the antenna port. Comprehensive details on the computed SAR peak values at the target frequencies are provided in Table 1, which also includes 1 g SAR values to facilitate comparisons with prior studies. The results reveal that the simulated maximum 1-g averaged SAR values are 84.8 W/kg and 123.7 W/kg at 1.4 and 2.45 GHz, respectively.

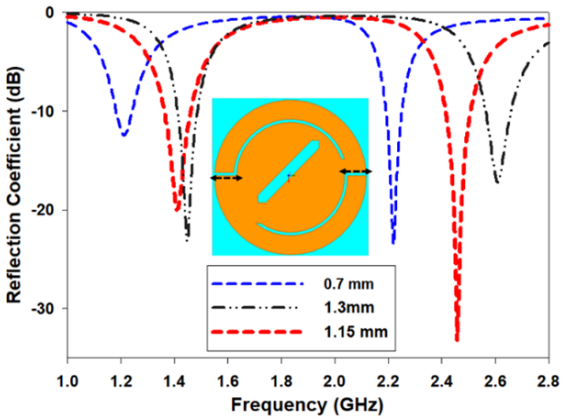


Fig. 8. Effects of the open-end slots length

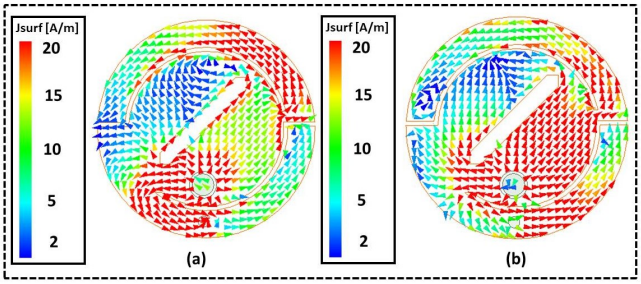


Fig. 9. Current distributions on the patch layer at (a) 1.4 and (b) 2.45 GHz.

Meanwhile, the SAR values for the 10 g standard are 4.77 W/kg and 6.07 W/kg at 1.4 GHz and 2.45 GHz, respectively. Subsequently, the corresponding maximum input power levels for both frequencies are calculated and are presented in Table 1. Notably, these values indicate significantly lower power levels than the typical power used for implants according to the ITU-R SM.2153-8 standard [22]. These findings affirm the appropriateness and safety of the proposed antenna design for operation within the human body.

## III. EXPERIMENTS AND RESULTS

Once the desired results are achieved, the antenna is meticulously fabricated and embedded within a biocompatible capsule, as depicted in Fig. 11 (a). Dummy components, including sensors, batteries, and a PCB, are integrated into the capsule device. For measurement purposes, the capsule device is equipped with a coaxial cable passage hole, precisely matching the cable conductor's diameter. To ensure the real test environment, the measurements of the antenna ($S_{11}$) and radiation performance were conducted with the capsule placed inside a container filled with minced pork meat, the size of this container is 250 x 250 x 150 $mm^3$ with depth 75mm. The $S_{11}$ measurements were done using a vector network analyzer (VNA) (Series 8722ES). Fig. 12 compared the measured and simulated antenna ($S_{11}$) at both frequency bands. Notably, the experimental results confirm the applicability of the antenna with the resonances falling within the target WMTS 1.4 GHz and ISM 2.45 GHz bands. Any observed discrepancies can be attributed to variations in the dielectric properties between

© 2024 IEEE. Personal use is permitted, but republication/redistribution requires IEEE permission. See https://www.ieee.org/publications/rights/index.html for more information.

This article has been accepted for publication in IEEE Sensors Journal. This is the author's version which has not been fully edited and content may change prior to final publication. Citation information: DOI 10.1109/JSEN.2024.3374817



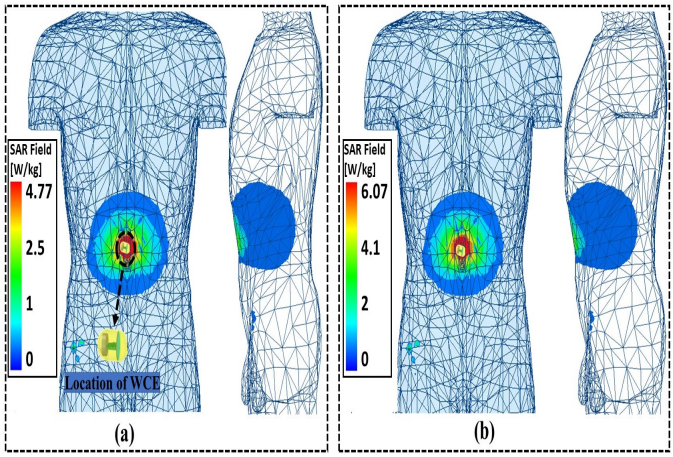


Fig. 10. Computed SAR distributions at (a) 1.4 GHz and (b) 2.45 GHz averaged over 10 g of tissues.

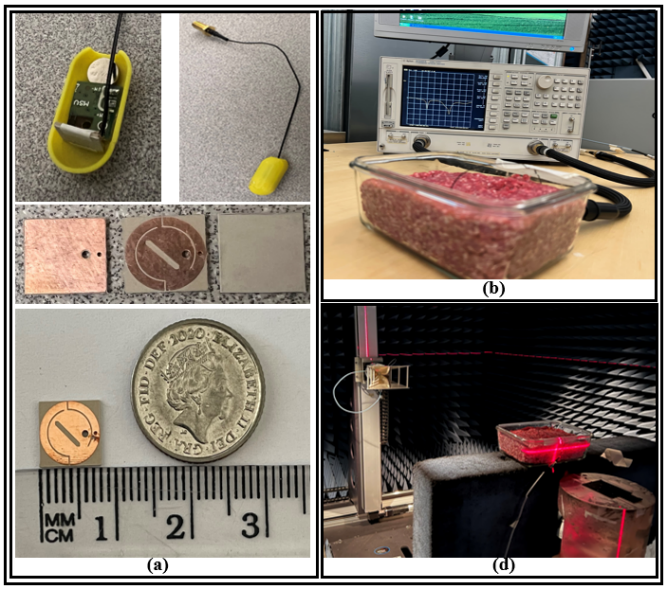


Fig. 11. (a) Fabricated antenna prototype before and after capsule assembly. Experimental setup with an antenna embedded inside minced pork: (b) $S_{11}$ test, (c) far-field test in the anechoic chamber.

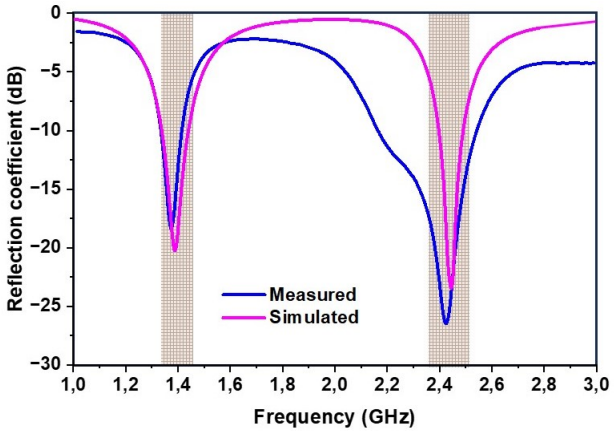


Fig. 12. Simulated and measured $S_{11}$.

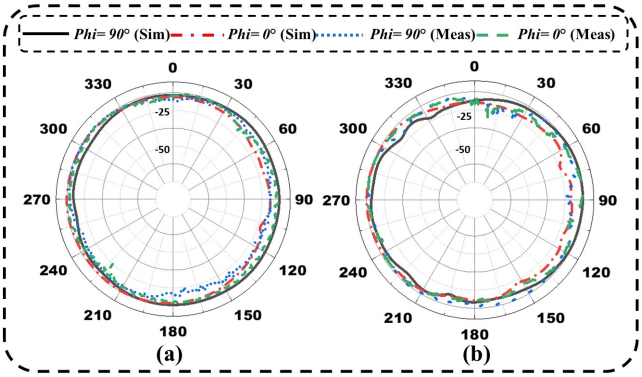


Fig. 13. Simulated and measured antenna radiation patterns at (a) 1.4 GHz and (b) 2.45 GHz.

the heterogeneous tissue materials used in the simulations and experiments. Additionally, the antenna fabrication tolerances including the gap between the substrate and the superstrate may lead to antenna performance variations.

In Fig. 13, the suggested antenna's simulated and measured radiation patterns at 1.4 GHz and 2.45 GHz are displayed. The measurements were conducted in an anechoic chamber. The experimental setup involved the antenna's placement at the center of a container filled with minced pork meat, facilitating the handling process. The antenna and the reception horn antenna were mounted at a distance of three meters. One antenna is terminated with a 50 Ω load, while the other is attached to a spectrum analyzer for the duration of the measurements. The antenna was systematically rotated with a sweeping angle of 2 degrees, while the horn antenna remained stationary. As shown in Fig. 13, the antenna demonstrates omnidirectional patterns at both frequencies. This feature holds significant importance to ensure comprehensive coverage and dependable communication, regardless of the changing orientation of the capsule device within the GI tract. In the simulations inside the stomach of the realistic human model, the antenna shows peak realized gains of -29.4 and -30.4 dBi at 1.4 and 2.45 GHz, respectively. The measurements inside the minced pork meat exhibit peak gain values of -27.6 and 28.7 at 1.4 and 2.45 GHz, which are almost identical to those simulated. The discrepancies in the results are associated with the factors mentioned before. To underscore the novelty and benefits of the proposed study, a comprehensive comparison is conducted with previously reported dual-band implantable antennas, as presented in Table 3. The analysis reveals several notable advantages of the suggested implantable antenna, particularly in terms of the antenna dimensions, implantation depth, and reduced SAR, setting it apart from other dual-band antenna.

## IV. Link Budget Analysis

The primary role of the antenna is to facilitate the transfer of data captured by the implant to the data-gathering device. Therefore, before implementing the antenna in practical implants, it is essential to evaluate its communication capability. This can be done through a link budget (LM) analysis that takes into account the antenna free space losses, path loss exponent, antenna mismatches, cable losses, and shadowing

© 2024 IEEE. Personal use is permitted, but republication/redistribution requires IEEE permission. See https://www.ieee.org/publications/rights/index.html for more information.

This article has been accepted for publication in IEEE Sensors Journal. This is the author's version which has not been fully edited and content may change prior to final publication. Citation information: DOI 10.1109/JSEN.2024.3374817



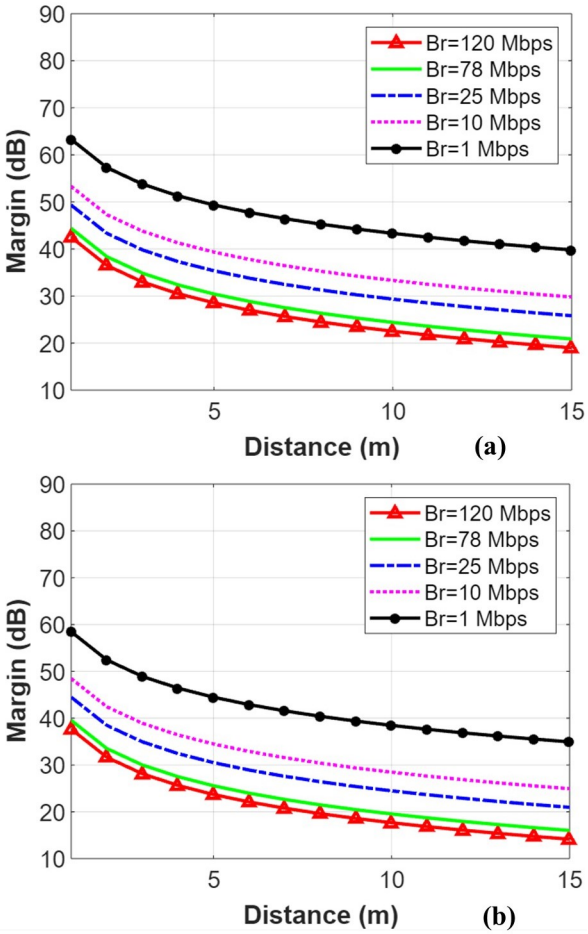


Fig. 14. LM as a function of distance (*d*) at (a) 1.4 GHz and (b) 2.45 GHz.

effects [23]. To ensure reliable communication, the LM must remain above 0 dB [16]. In this study, an LM of 20 dB is considered to ensure seamless communication. Theoretical evaluation of the antenna's communication capabilities was conducted using the Friis equations as provided in [2]. In this analysis, the suggested antenna is considered as a transmitting antenna, and the dipole antenna serves as the receiving antenna. To record the data, The receiving and transmitting antennas have a varying distance between them. The implantable antenna kept a transmitted input power of -16 dBm. (25 $\mu$W). The antenna's required power (Rr) is calculated as

$$R_r(dB) = \frac{E_b}{N_0} + KT_0 + R_r \tag{1}$$

In this context, $R_r$ represents the minimum needed power (dB), $T$ is the temperature (293K), $E_b/N$ represents denotes the PSK modulation value at 9.6 dB, $K$ represents the Boltzmann constant ($1.38e^{-23}$), and $B_r$ represents the bit rate [24]. Furthermore, the antenna's available power ($R_a$) is calculated as

$$R_a(dB) = (P_t + G_t + G_r - PL - L_p) \tag{2}$$

TABLE II
LINK BUDGET PARAMETERS

| Specification | Variable | Value |
|---|---|---|
| Resonant frequency (GHz) | $f$ | 1.4/2.45 |
| Transmitter Power (dBm) | $P_a$ | -16 |
| Path loss exponent | $\gamma$ | 1.5 |
| Temperature (Kelvin) | $T$ | 273 |
| Transmitter antenna gain (dBi) | $G_a$ | Tissue dependent |
| Receiving antenna gain (dBi) | $G_b$ | 2 |
| Free space loss (dB) | $L$ | Distance dependent |
| Available power (dB) | $A_p$ | Distance dependent |
| Required power (dB) | $R_p$ | Adaptive (Bit rate) |
| Margin (dB) | $A_p - R_p$ | Fig.15 |

In this context, $R_a$ represents the available power, $P_t$ represents the transmitter power of the dual-band antenna, $G_t$ represents the gain of the transmitter antenna, $G_r$ represents the gain of the receiver antenna, $PL$ represents the polarization loss factor, and $L_p$ represents the path loss between the transmitter antenna and receiver antenna. The latter can be calculated as

$$L_p(\text{dB}) = 20\log_{10}\left(\frac{4\pi d}{\lambda}\right) + 10\gamma\log_{10}\left(\frac{d}{d_0}\right) + S_e \tag{3}$$

where $d$ is the distance between transmitter and receiver antennas, $\gamma$ represents the path loss exponent and $S_e$ accounts for the effect of shadowing with the standard deviation of $\sigma$. All required parameters for (LM) analysis are provided in Table 2. Five distinct bit rates (1, 10, 25, 78, and 120 Mbps) were considered in the link budget calculation at operating frequencies of 1.4 and 2.45 GHz. The corresponding transmission ranges for these data rates are depicted in Fig. 14. The findings indicate that the suggested antenna can consistently transmit data over distances exceeding 10 meters while maintaining a 15 dB margin for both frequencies. With an LM of 15 dB, the antenna can transmit data over distances exceeding 15 meters at a rate of 120 Mbps for both frequencies. These findings affirm the suitability of the suggested antenna for biotelemetry applications.

## V. CONCLUSION

This article illustrates the design of a compact dual-band antenna system intended for the WCE system. Through a range of design features, the system aims to achieve miniaturization while also providing dual-band capabilities. These features include a shorting pin, open-ended slots, semi-circular slots, and a middle slot on the radiator patch. This antenna design has a compact size of 42.69 $mm^3$. This device operates in the WMTS 1.4 GHz as well as the ISM 2.4 GHz bands, which were successfully achieved based on the evaluation

© 2024 IEEE. Personal use is permitted, but republication/redistribution requires IEEE permission. See https://www.ieee.org/publications/rights/index.html for more information.

This article has been accepted for publication in IEEE Sensors Journal. This is the author's version which has not been fully edited and content may change prior to final publication. Citation information: DOI 10.1109/JSEN.2024.3374817



TABLE III
COMPARISON WITH STATE-OF-THE-ART DUAL-BAND IMPLANTABLE ANTENNAS

| Ref | Size ($\lambda g^3$) | Size ($mm^3$) | Frequency (MHz) | implantation depth (mm) | Peak gain (dBi) | SAR (W/kg) 1-g | SAR (W/kg) 10-g |
|---|---|---|---|---|---|---|---|
| [25] | 0.0059 | 15 × 15 ×15 | 2450<br>5800 | 30 | -18.5 | 1101.7<br>1135.8 | 276<br>284 |
| [26] | 0.00203 | 16 × 16 × 2.4 | 1400<br>2450 | 2 | -13.25<br>-11.3 | —<br>— | —<br>— |
| [27] | 0.0021 | 9.8 × 9.8 × 1.27 | 2450 | 3 | 33 | 486 | 90 |
| [28] | 0.00034 | $\pi \times (5.1)^2 \times 1.27$ | 1400<br>2450 | 3 | -32<br>-31.6 | 702<br>781 | 88.5<br>88.8 |
| [29] | 0.00153 | 8.5 × 8.5 × 1.27 | 2400<br>4800 | 42 | -26<br>-8.8 | 207<br>137.1 | 24.1<br>28.8 |
| [30] | 0.00066 | $\pi \times (4.8)^2 \times 0.13$ | 1400<br>2450 | 3 | -24.5<br>-20.6 | 294<br>409 | 61.9<br>83.2 |
| [31] | 0.0022 | 10 × 10 × 1.27 | 2450 | 4 | -27.2 | — | — |
| [32] | 0.00047 | 10 × 10 × 0.635 | 1400<br>2400 | 4 | -37<br>-21 | 215<br>565 | 38.75<br>694.7 |
| [33] | 0.00053 | 11 × 11 × 1.28 | 1400<br>2400 | 3 | -25.7<br>-39.9 | —<br>— | —<br>— |
| **This Work** | **0.00014** | **8.2 × 8.2 × 0.635** | **1400<br>2450** | **75** | **-29.4<br>-30.4** | **84.8<br>123.7** | **6.07<br>4.77** |

of simulation and measurement results using both a human body phantom and minced pork. Additionally, the capsule device with a radius of 6.2 mm and length of 18.9 mm was designed to assess the antenna performance in a real device-like environment. Considering the capsule's deep location, the proposed antenna achieves gain values of -29.4 dBi at 1.4 GHz and -30.4 dBi at 2.45 GHz, respectively. Furthermore, the safety of the antenna was evaluated by IEEE SAR regulations. The 10-g SAR values are 4.77 W/kg and 6.07 W/kg at 1.4 GHz and 2.45 GHz.This antenna design exhibits promising potential as a suitable choice for implantable medical devices in capsule endoscopy applications.

## REFERENCES


[1] A. Iqbal, M. Al-Hasan, I. B. Mabrouk, and T. A. Denidni, "Deep-implanted mimo antenna sensor for implantable medical devices," *IEEE Sensors Journal*, vol. 23, no. 3, pp. 2105–2112, 2023.

[2] W. Wang, X.-W. Xuan, W.-Y. Zhao, and H.-K. Nie, "An implantable antenna sensor for medical applications," *IEEE Sensors Journal*, vol. 21, no. 13, pp. 14 035–14 042, 2021.

[3] R. Kumar and S. Singh, "Cpw fed conformal pifa design for implantable iomt devices with wideband performance," *IEEE Sensors Journal*, 2023.

[4] T. Govindan, S. K. Palaniswamy, M. Kanagasabai, S. Kumar, R. Agarwal, R. Kumar, and D. Panigrahy, "Design and analysis of a conformal mimo ingestible bolus sensor antenna for wireless capsule endoscopy for animal husbandry," *IEEE Sensors Journal*, 2023.

[5] G. Bebis, R. Boyle, B. Parvin, D. Koracin, S. Wang, K. Kyungnam, B. Benes, K. Moreland, C. Borst, S. DiVerdi *et al.*, *Advances in Visual Computing: 7th International Symposium, ISVC 2011, Las Vegas, NV, USA, September 26-28, 2011. Proceedings, Part I*. Springer, 2011, vol. 6938.

[6] C.-M. Lee, T.-C. Yo, F.-J. Huang, and C.-H. Luo, "Bandwidth enhancement of planar inverted-f antenna for implantable biotelemetry," *Microwave and Optical Technology Letters*, vol. 51, no. 3, pp. 749–752, 2009.

[7] F. N. Alsunaydih, M. A. Ali, and M. R. Yuce, "Wireless capsule design and its locomotion and navigation within the body," in *Handbook of Biochips: Integrated Circuits and Systems for Biology and Medicine*. Springer, 2022, pp. 1013–1036.

[8] C. C. Poon, B. P. Lo, M. R. Yuce, A. Alomainy, and Y. Hao, "Body sensor networks: In the era of big data and beyond," *IEEE reviews in biomedical engineering*, vol. 8, pp. 4–16, 2015.

[9] P. D. Bradley, "An ultra low power, high performance medical implant communication system (mics) transceiver for implantable devices," in *2006 IEEE Biomedical Circuits and Systems Conference*. IEEE, 2006, pp. 158–161.

[10] U. Banerjee, A. Karmakar, A. Saha, and P. Chakraborty, "A cpw-fed compact monopole antenna with defected ground structure and modified parasitic hilbert strip having wideband circular polarization," *AEU-International Journal of Electronics and Communications*, vol. 110, p. 152831, 2019.

[11] X. Tang, H. Wong, Y. Long, Q. Xue, and K. Lau, "Circularly polarized shorted patch antenna on high permittivity substrate with wideband," *IEEE Transactions on Antennas and Propagation*, vol. 60, no. 3, pp. 1588–1592, 2011.

[12] R. Kangeyan and M. Karthikeyan, "Miniaturized meander-line dual-band implantable antenna for biotelemetry applications," *ETRI Journal*, 2023.

[13] K. Yeap, C. Voon, T. Hiraguri, and H. Nisar, "A compact dual-band implantable antenna for medical telemetry," *Microwave and Optical*


© 2024 IEEE. Personal use is permitted, but republication/redistribution requires IEEE permission. See https://www.ieee.org/publications/rights/index.html for more information.

This article has been accepted for publication in IEEE Sensors Journal. This is the author's version which has not been fully edited and
content may change prior to final publication. Citation information: DOI 10.1109/JSEN.2024.3374817



*Technology Letters*, vol. 61, no. 9, pp. 2105–2109, 2019.
[14] T. Karacolak, A. Z. Hood, and E. Topsakal, "Design of a dual-band implantable antenna and development of skin mimicking gels for continuous glucose monitoring," *IEEE transactions on microwave theory and techniques*, vol. 56, no. 4, pp. 1001–1008, 2008.
[15] F. Faisal and H. Yoo, "A miniaturized novel-shape dual-band antenna for implantable applications," *IEEE Transactions on Antennas and Propagation*, vol. 67, no. 2, pp. 774–783, 2018.
[16] S. A. A. Shah and H. Yoo, "Scalp-implantable antenna systems for intracranial pressure monitoring," *IEEE Transactions on Antennas and Propagation*, vol. 66, no. 4, pp. 2170–2173, 2018.
[17] Y. Cho and H. Yoo, "Miniaturised dual-band implantable antenna for wireless biotelemetry," *Electronics Letters*, vol. 52, no. 12, pp. 1005–1007, 2016.
[18] "Tissue properties database," http://niremf.ifac.cnr.it/tissprop/, accessed on October 27, 2023.
[19] R. B. Waterhouse and R. Waterhouse, "Small microstrip patch antennas," *Microstrip Patch Antennas: A Designer's Guide*, pp. 197–276, 2003.
[20] D. Uzer and S. GÜLTEKİN, "An investigation of shorting pin effects on circular disc microstrip antennas," *International Journal of Applied Mathematics, Electronics and Computers*, vol. 3, no. 3, pp. 218–222, 2015.
[21] W. H. Bailey, R. Bodemann, J. Bushberg, C.-K. Chou, R. Cleveland, A. Faraone, K. R. Foster, K. E. Gettman, K. Graf, T. Harrington *et al.*, "Synopsis of ieee std c95. 1™-2019 "ieee standard for safety levels with respect to human exposure to electric, magnetic, and electromagnetic fields, 0 hz to 300 ghz"," *IEEE Access*, vol. 7, pp. 171 346–171 356, 2019.
[22] I. T. Union. (2021) Recommendation itu-r sm.2153-8. [Online]. Available: https://www.itu.int/pub/R-REP-SM.2153-8-2021
[23] I. Gani and H. Yoo, "Multi-band antenna system for skin implant," *IEEE Microwave and Wireless Components Letters*, vol. 26, no. 4, pp. 294–296, 2016.
[24] A. Iqbal, M. Al-Hasan, I. B. Mabrouk, and T. A. Denidni, "Capsule endoscopic mimo antenna with radiation pattern and polarization diversity," *IEEE Transactions on Antennas and Propagation*, vol. 71, no. 4, pp. 3146–3154, 2023.
[25] V. Kaim, B. K. Kanaujia, and K. Rambabu, "Quadrilateral spatial diversity circularly polarized mimo cubic implantable antenna system for biotelemetry," *IEEE Transactions on Antennas and Propagation*, vol. 69, no. 3, pp. 1260–1272, 2020.
[26] R. B. Green, M. Hays, M. Mangino, and E. Topsakal, "An anatomical model for the simulation and development of subcutaneous implantable wireless devices," *IEEE Transactions on Antennas and Propagation*, vol. 68, no. 10, pp. 7170–7178, 2020.
[27] Z. Xia, H. Li, Z. Lee, S. Xiao, W. Shao, X. Ding *et al.*, "A wideband circularly polarized implantable patch antenna for ism band biomedical applications," *IEEE Transactions on Antennas and Propagation*, vol. 68, no. 3, pp. 2399–2404, 2019.
[28] L.-J. Xu, Z.-J. Chu, L. Zhu, J.-P. Xu, and Z. Duan, "Design and analysis of dual-band implantable antennas based on effective relative permittivity calculation," *IEEE Transactions on Antennas and Propagation*, vol. 69, no. 5, pp. 2463–2472, 2020.
[29] S. S. Mosavinejad, P. Rezaei, and A. A. Khazaei, "A miniaturized and biocompatible dual-band implantable antenna for fully-passive wireless signal monitoring," *AEU-International Journal of Electronics and Communications*, vol. 154, p. 154303, 2022.
[30] M. S. Singh, S. Roy, J. Ghosh, U. Chakraborty, S. Ghosh, and A. Sarkhel, "Design and analysis of compact dual-band antenna system for scalp and skin implantation," *Progress In Electromagnetics Research C*, vol. 125, pp. 1–13, 2022.
[31] Z.-J. Yang, S.-Q. Xiao, L. Zhu, B.-Z. Wang, and H.-L. Tu, "A circularly polarized implantable antenna for 2.4-ghz ism band biomedical applications," *IEEE Antennas and Wireless Propagation Letters*, vol. 16, pp. 2554–2557, 2017.
[32] R. Kangeyan and M. Karthikeyan, "Miniaturized meander-line dual-band implantable antenna for biotelemetry applications," *ETRI Journal*, 2023.
[33] A. Valanarasi and R. Dhanasekaran, "Optimum band shaped miniature implantable antennas for telemetry applications," *IEEE Transactions on Antennas and Propagation*, vol. 69, no. 1, pp. 55–63, 2021.

**Abdullah Alshammari** (Student Member, IEEE) was born in Riyadh, Saudi Arabia, in 1989. He received a B.Sc. degree in communication and software engineering from Al-Balqa Applied University, Jordan, in 2015. He received an M.Sc. degree in microelectronic and communication engineering from Northumbria University, United Kingdom, in 2020.

He is currently pursuing a Ph.D. degree in antenna and propagation at Durham University, United Kingdom. His research interests include biomedical implantable antennas, wireless capsule endoscopy, flexible antennas.

**Amjad Iqbal** (Member, IEEE) received the B.S. degree in electrical engineering from COMSATS University, Islamabad, Pakistan, in 2016, the M.S. degree in electrical engineering from the CECOS University of IT and Emerging Sciences, Peshawar, Pakistan, in 2018, and the Ph.D. degree in engineering from Multimedia University, Selangor, Malaysia, in 2021.

He worked as a Laboratory Engineer with the Department of Electrical Engineering, CECOS University Peshawar, Peshawar, from 2016 to 2018. His research interests include printed antennas, flexible antennas, implantable antennas, multiple-input and multiple-output (MIMO) antennas, dielectric resonator antennas, wireless power transfer, and synthesis of microwave components.

**Abdul Basir** (Member, IEEE) was born in Khyber Pakhtunkhwa, Pakistan, in 1989. He received the B.Sc. degree in telecommunication engineering from the University of Engineering and Technology, Peshawar, Pakistan, in 2015,and the Ph.D. degree in electronic engineering from Hanyang University, Seoul, South Korea,in 2021. He is currently a Postdoctoral Researcher with Hanyang University. His research interests include implantable antennas and systems, biomedical circuits, wearable antennas, MIMO communication, metamaerial, dielectric resonator antennas, reconfigurable antennas, long-range wireless power transfer, and wireless charging of biomedical implants. He received the Silver Prize for the Best Student Paper Awards in Student Paper Contests 2018 and 2019, IEEE Seoul Section. His collaborated paper received the Best Paper Award 2019 by IEEE AP/MTT/EMC Joint Chapter Malaysia. He received the Third Prize for the Best Student Paper Completion 2018 by the Korea Communications Agency (KCA) and the Korean Institute of Electromagnetic Engineering and Science (KIEES).

© 2024 IEEE. Personal use is permitted, but republication/redistribution requires IEEE permission. See https://www.ieee.org/publications/rights/index.html for more information.

This article has been accepted for publication in IEEE Sensors Journal. This is the author's version which has not been fully edited and content may change prior to final publication. Citation information: DOI 10.1109/JSEN.2024.3374817



**Roy B. V. B. Simorangkir** (Member, IEEE) holds a B.S. degree in Telecommunication Engineering from the Institut Teknologi Bandung, Indonesia (2010), an M.S. degree in Electrical and Electronic Engineering from Yonsei University, South Korea (2014), and a Ph.D. in Electronic Engineering from Macquarie University, Australia (2018). After completing his Ph.D., he pursued postdoctoral research at Macquarie University, Institute of Electronics and Telecommunications of Rennes, France, and Tyndall National Institute, Ireland. Dr. Simorangkir is currently an Assistant Professor in the Department of Engineering at Durham University, UK, where he specializes in the development of unconventional materials-based antennas and sensors for next-generation wireless communication and sensing systems. He has published over 60 refereed research papers in this field, including award-winning work. He has also taken on leadership roles at major international conferences and received recognition as an outstanding reviewer for esteemed journals, notably from 2021 to 2023 for the IEEE Transactions on Antennas and Propagation

**Ismail Ben Mabrouk** (Senior Member, IEEE) received the B.A.Sc. and M.A.Sc. degrees in electrical engineering from the University of Lille, Lille, France, in 2006 and 2007, respectively, and the Ph.D. degree in electrical engineering from the University of Quebec, Montreal, QC, Canada, in 2012.

From 2007 to 2009, he was with Huawei Technologies, Paris, France. In 2012, he joined the Wireless Devices and Systems (WiDeS) Group, University of Southern California, Los Angeles, CA, USA. He is currently an Assistant Professor with Durham University, Durham, U.K. His research activities have been centered on antenna design at the millimeter-wave and THz frequencies, propagation studies for multiple-input and multiple-output (MIMO) systems, deep learning, and wireless body area network for medical applications.

Dr. Mabrouk was a recipient of the Abu Dhabi Award for Research Excellence (AARE) in 2018.

© 2024 IEEE. Personal use is permitted, but republication/redistribution requires IEEE permission. See https://www.ieee.org/publications/rights/index.html for more information.

Durham University
Durham Research Online

**Citation on deposit:** Alshammari, A., Iqbal, A., Basir, A., Simorangkir, R. B. V. B., & Mabrouk, I. B. (2024). Ultra-Miniaturized Dual-Band Implantable Antenna for Wireless Capsule Endoscopy. IEEE Sensors Journal, 24(9), 15210-15218. https://doi.org/10.1109/jsen.2024.3374817

**For final citation and metadata, visit Durham Research Online URL:**
https://durham-repository.worktribe.com/output/2334336

**Copyright statement:** This accepted manuscript is licensed under the Creative Commons Attribution 4.0 licence.
https://creativecommons.org/licenses/by/4.0/